Boundary-Layer Meteorology Vol. 74, No. 4, pp. 321–340, 1995
re-paginated final version of manuscript

A COSPECTRAL CORRECTION MODEL FOR MEASUREMENT OF TURBULENT NO_2 FLUX

W. EUGSTER
Institute of Geography, Climatology and Meteorology, University of Bern, Switzerland

W. SENN
Institute of Informatics and Applied Mathematics, University of Bern, Switzerland

(Received 29 September, 1994)

Abstract. A correction model for eddy correlation flux measurements is developed and applied to nitrogen dioxide flux measurements obtained from a SOLENT sonic anemometer and a Scintrex Luminox LMA-3 analyser for NO_2. Four field campaigns were carried out near the village of Merenschwand in Central Switzerland from which two were selected for further analysis in this paper. The need for the correction of measured eddy covariance fluxes arises due to the damping loss of the NO_2 analyser at high frequencies. This damping loss is described by an analogy to inductance in an electronical alternating current circuit. The independent variables in the correction model are: z (measuring height above zero-plane displacement), $\overline{u}$ (mean horizontal wind speed), ζ (Monin-Obukhov stability parameter), f (natural frequency) and inductance L. The value for inductance L can be derived from spectral and cospectral analysis. The theoretical cospectrum of an ideal measurement is taken from Kaimal *et al.* (1972) and extended with a damping term in order to describe the real measurements of the cospectrum. The inductance L of the LMA-3 with a $\frac{1}{4}''$ teflon aspiration tube of 5 m length lies in the order of 0.30 to 0.35 for the dataset from Merenschwand. With this inductance, a correction factor of 1.17 in August/September 1992 and of 1.18 in May 1993 was determined for the NO_2 flux maxima during daytime. The range of the correction factor is 1.05 to 1.31 for the mean daily cycles of both datasets.

1. Introduction

The turbulent fluxes of momentum and heat are no longer difficult to measure thanks to high-speed sonic anemometers and diverse publications on the measuring errors and averaging problems of these measurements (e.g., Kaimal *et al.*, 1968; Kaimal and Gaynor, 1991; Businger, 1986; Grant and Watkins, 1989; Hicks and McMillen, 1988; Skupniewicz *et al.*, 1989). The eddy correlation method commonly used to measure these turbulent fluxes can also be used to measure dry deposition and fluxes of scalars like water vapor or trace gases. Hicks and McMillen (1988) gave an overview of how dry deposition can be measured using imperfect sensors in non-ideal terrain. They list the requirements for the gradient method, the Bowen ratio approach and the eddy correlation technique. The latter is the preferred method because it does not require an assumption regarding eddy diffusivities. However, fast-response sensors are required for the eddy correlation technique; this limits its application to very few chemical species. During a joint project with the Federal Institute of Agricultural Research, Liebefeld (Switzerland), eddy correlation fluxes of NO_2 were measured with a Scintrex Luminox LMA-3 NO_2 analyser, a widely used instrument, in combination with a Solent Sonic Anemometer, near the village of Merenschwand in the lower Reuss valley.

In addition to the known problems of high frequency noise (Kaimal and Gaynor, 1991, Hicks and McMillen, 1988) and high frequency loss due to instrumental cut-off (Panofsky and Dutton, 1984), the problem of instrumental damping of the LMA-3 and its influence on the flux measurements was thoroughly investigated. Similar works have been published by Leuning and Moncrieff (1990), where the damping effects in a CO_2 analyser

Table I. Measuring heights and sectoral fetches. In August / September 1992 the zero-displacement height d was determined from profile and eddy correlation measurements such that the non-dimensional profile (Monin and Obukhov, 1954) for momentum, ϕ_m was unity with neutral stratification, $\phi_m(0) = 1$.

	August/September 1992	May 1993
$z + d$	2.59 m	2.00 m
d	0.48 m	0.02 m
fetch $\geq 100 \cdot z$	155° – 329°	180° – 330°
$30 \cdot z \leq$ fetch $< 100 \cdot z$	329° – 068°	330° – 058°
	110° – 155°	098° – 180°
data excluded	068° – 110°	058° – 098°

are discussed using a somewhat different approach, and Moore (1986) gives a detailed theoretical overview of where damping could occur in an eddy correlation measuring system. Here we present a new correction model for eddy correlation nitrogen dioxide flux measurements.

2. Experimental Details

2.1. The Measuring Site

The village of Merenschwand is located in the lower Reuss valley at an altitude of 385 m asl. The plain bottom of the valley is slightly inclined (0.06°) towards the NNW; the width of the valley bottom at this location is about 2.5 km. Land use exhibits a changing pattern of agriculture, hedges and natural protected areas. The measuring system was set up in a natural protected area 2.59 m above ground in August and September 1992, and at 2.00 m in May 1993. The fetch was at least 260 m in the mean wind direction (NNW). The northeastern border of the natural protected area is marked by a hedge 3 to 5 m tall. The local vegetation consists of grass, herbeous plants and scattered shrubs which grow up in mid-June and are cut in October. An overview of the fetch criterion according to Businger (1986) is given in Tab. I. Due to the changing land-use pattern and some obstacles to the south, Merenschwand is a typical case of 'non-ideal' terrain (Hicks and McMillen, 1988). It was chosen because this part of the Reuss valley is a nationally protected site surrounded by extensively cultivated agricultural land, so that atmospheric deposition of nitrogenous compounds is of great importance (Ellenberg, 1990). The aim was to quantify the dry deposition of NO_2 by eddy correlation measurements, and of other nitrogeneous species (NH_3, NH_4^+, HNO_3, NO_3^-, PAN, NO, HONO, NO_2^- and N_2O_5) using gradient methods or bulk transfer methods. Wet deposition (NH_4^+ and NO_3^-) was also measured. The results of all deposition measurements will be published elsewhere (Hesterberg *et al.*, 1995).

2.2. The Instruments

The Solent sonic anemometer used in this study was set up in calibrated mode with a data output rate of 20.83 Hz. The wind speeds from all three transducer pairs were internally averaged from 8 ultrasonic shots per pair. The results were then transformed

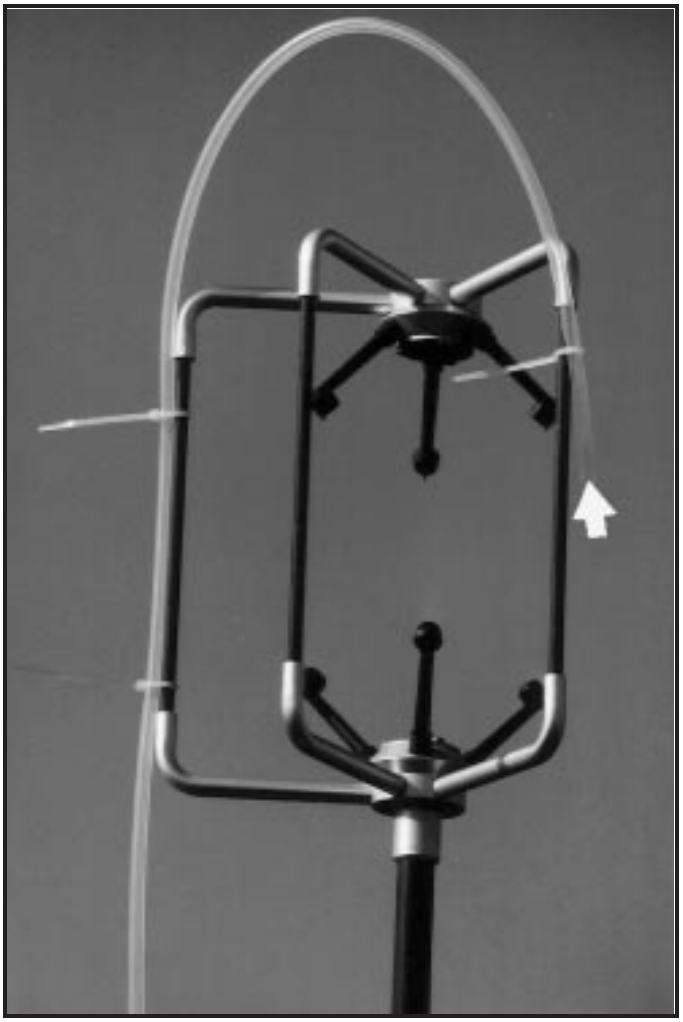

Figure 1. The sensor head of the sonic anemometer and the attached teflon tube for the NO_2 measurements.

into perpendicular x, y and z-coordinates and calibrated according to the manufacturer's calibration list. From the sonic anemometer's head frame (Fig. 1) a $\frac{1}{4}''$ teflon tube 5 m long was connected to the NO_2 analyser Luminox LMA-3. This approach offers the advantage of minimising the spatial separation between the wind measurements and the chemical measurements. Moreover, the low flow rate of the air pump (2.2 ℓmin^{-1}; Hesterberg, 1994) does not influence the wind measurements significantly when the air probe is taken on the leeward side of the sonic anemometer's head. A disadvantage of this small air flow rate seems to be that even in short tubes the air flow is not necessarily turbulent ($Re \approx$ 600), which is a primary cause of the high frequency loss in the measuring system. Another systematic error is introduced by the wet chemical reaction chamber of the LMA-3, where NO_2 from the air probe reacts with Luminol liquid. This seems to be a second source of the damping caused by the LMA-3 instrument. This damping has to be corrected, e.g. with the correction model proposed in this paper.

Table II. Notations used in the formulas.

Symbol	Description
c_{NO_2}	concentration of NO_2
f	natural frequency
n	normalized frequency, $n = fz/\overline{u}$
$\overline{u}$	mean horizontal wind speed along the mean wind direction
w	vertical wind speed
z	measuring height above zero-plane displacement
L	inductance
R	resistance
T_v	virtual temperature measured with a sonic anemometer
ζ	Monin-Obukhov stability parameter
θ	potential temperature
ξ	fraction of theoretical covariance which can be measured with an imperfect sensor
ω	cyclic frequency, $\omega = 2\pi f$
$Co_{x,y}(f)$	cospectral density at frequency f
$Q_{x,y}(f)$	spectral density of the quadrature spectrum at frequency f
$S_x(f)$	spectral density at frequency f

2.3. THE DATA ACQUISITION SYSTEM AND DATA SET

The analog signal of the Luminox LMA-3 was attached to one of the 5 internal analog-to-digital converters of the Solent sonic anemometer. The sampling rate of these A/D converters was 10.41 Hz, but the output in data blocks occurred at the same rate as the wind measurements (20.83 Hz). The digital data from the RS-422 serial port on the sonic anemometer were guided to a nearby shelter using a 250 m serial cable. There the signal was converted from RS-422 to RS-232 protocol, which was connected to a serial port on a SUN workstation. At the workstation the data were continuousely recorded and split into files with 75,600 measured values each. Within the UNIX environment, a simultaneous calculation of preliminary fluxes and mean values was carried out to control the measurements. The data set was therefore interrupted only by calibration passes (usually every second day), and technical break-downs in the system. Data exist from four field phases (June 1992, August/September 1992, January/February 1993 and May 1993) from which August/September 1992 and May 1993 were selected for the analyses in this paper. The June 1992 data are not included since there were some experimental uncertainties with the positioning of the instruments in the field, while in January/February 1993 there were much higher concentrations of NO_2, which meant that another measuring range of the instrument (0–200 ppb instead of 0–20 ppb) had to be selected. The NO_2 data were calibrated according to the calibration passes carried out in the field. The coordinates of the wind vectors were transformed to obtain $\overline{u}$ in the direction of the streamlines of the mean flow (Zeman and Jensen, 1987).

3. Theory

3.1. Statistical Preliminaries

The auto-spectrum of a time series $x(t)$ is defined by $S_x(f) = \frac{1}{\pi}\int_{-\infty}^{\infty} R_x(\tau)\cdot e^{2\pi i f\tau}d\tau$, where $R_x(\tau) = E\{x'(t)\cdot x'(t+\tau)\}$ denotes the autocorrelation function of $x(t)$. As usual, we write the time series x as $x(t) = \overline{x} + x'(t)$, with mean $\overline{x}$ and deviation $x'(t)$. Using the inverse Fourier transform $R_x(\tau) = \frac{1}{2}\int_{-\infty}^{\infty} S_x(f)e^{-2\pi i f\tau}df$, the variance $\sigma_x^2 = \overline{x'^2} = E\{x'^2\}$ of x may be expressed in terms of $S_x(f)$ according to

$$\overline{x'^2} = R_x(0) = \int_0^{\infty} S_x(f)df \ . \tag{1}$$

If the Fourier transform of the time series $x(t)$ is concentrated on one single frequency f_1, i. e. if $x(t) = \text{const}\cdot e^{2\pi i f_1 t}$, Eq. 1 reduces to

$$\overline{x'^2} = S_x(f_1) \ . \tag{2}$$

Notice that in the case $x(t) = \text{const}\cdot(f_1)e^{2\pi i f_1 t}$, the autocorrelation function of x again has the form $R_x(\tau) = \text{const}\cdot e^{2\pi i f_1\tau}$, when averaged over a finite time-interval. * Comparing $R_x(\tau)$ with its inverse Fourier transform above, the terms $S_x(f)$ with $f \neq f_1$ vanish and Eq. 2 is established.

The cross-spectrum of two time series $x(t)$ and $y(t)$ is defined by $\Lambda_{x,y}(f) = \frac{1}{\pi}\int_{-\infty}^{\infty} R_{x,y}(\tau)\cdot e^{2\pi i f\tau}d\tau$, where $R_{x,y}(\tau) = E\{x'(t)\cdot y'(t+\tau)\}$ denotes the cross-correlation function of $x(t)$ and $y(t)$. The cross-spectrum is decomposed into cospectrum and quadrature spectrum according to $\Lambda_{x,y}(f) = Co_{x,y}(f) + iQ_{x,y}(f)$. Using the inverse Fourier transform together with symmetry/anti-symmetry arguments, the covariance $\overline{x'y'} = E\{x'(t)y'(t)\}$ of the two time series is calculated by

$$\overline{x'y'} = R_{x,y}(0) = \int_0^{\infty} Co_{x,y}(f)df \ . \tag{3}$$

Assuming that the Fourier transforms of x and y are each concentrated on a single frequency, say f_1 and f_2, with $x(t) = \text{const}\cdot e^{2\pi i f_1 t}$ and $y(t) = \text{const}\cdot e^{2\pi i f_2 t}$, the covariance reduces to

$$\overline{x'y'} = Co_{x,y}(f_2) \ \ (= Co_{y,x}(f_1)) \ . \tag{4}$$

Indeed, if $x(t) = \text{const}\cdot e^{2\pi i f_1 t}$ and $y(t) = \text{const}\cdot e^{2\pi i f_2 t}$, the cross-correlation function is calculated by $R_{x,y}(\tau) = \text{const}\cdot e^{2\pi i f_2\tau}$ when averaged over a fixed time-interval. Comparing with the Fourier representation of $R_{x,y}(\tau)$, one concludes that $Co_{x,y}(f) \neq 0$ for $f = f_2$ only.

The cospectrum is of particular interest for eddy correlation studies: If w denotes the vertical wind speed and θ the temperature, the covariance $\overline{w'\theta'}$ is interpreted as the turbulent flux and thus equates with the integral of the cospectrum from 0 to ∞.

Models of spectra can be found in Kaimal *et al.* (1972), Panofsky (1978), Højstrup (1981), Panofsky *et al.* (1982) and Claussen (1985). The models of cospectra used in this paper are adopted from Kaimal *et al.* (1972). The notations used here are given in Tab. II.

* As a convention, the constants abbreviated by const. do not need to be the same.

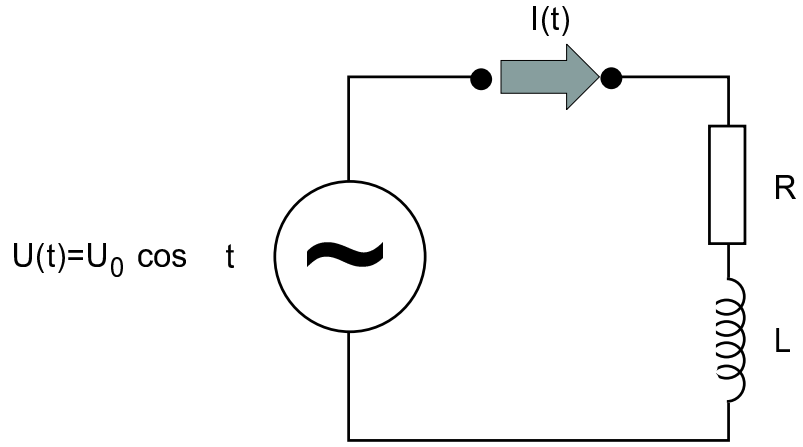

Figure 2. A circuit with inductance driven by an alternating electromotive force (see text for symbols).

3.2. THE DAMPING LAW - INDUCTANCE IN AN ALTERNATING-CURRENT CIRCUIT

All logarithmic spectra of the LMA-3 measurements showed a proportionality with $f^{-8/3}$ (Fig. 4.1) instead of $f^{-2/3}$ in the inertial subrange described by Kaimal *et al.* (1972)[†]. There seems to be an additional proportionality f^{-2} between the spectrum of sonic temperature and the damped measurement of NO_2 from the LMA-3. That this effect is not noise can also be seen in Fig. 4.1: the proportionality to f^{+1} coming from white noise (Kaimal and Gaynor, 1991) affects only frequencies above $n = 5$, while in the range $0.1 < n < 5$ there is a notable disparity between the spectrum of the temperature and the spectrum of the NO_2 time series. Vilá-Guerau de Arellano and Duynkerke (1987) show that NO_2 nearly behaves as a scalar in the lower surface layer. According to Panofsky and Dutton (1984) it could be expected that the spectra of any scalar, $fS_x(f)$, should have the same form when scaled by the variance of the time series, $\overline{x'^2}$. Moreover, noise is an addition to the real signal, while in the spectra from the LMA-3 (Fig. 4.1) there is a reduction of spectral density. The deficit of spectral density in this range can be explained by analogy to the following damping model taken from electronic circuitry. A similar approach, but with a gain function instead of electronic components in a current circuit, can be found in Moore (1986). Taking an analogy to electrical components has proven to be a valuable tool in plant physiology (e.g. resistance analogy) and could serve to facilitate understanding when a system gets more complicated, say when several components, such as resistances R, capacitors C and inductances L, are combined.

The simple circuit in Fig. 2 contains an inductance L and a resistance R, and is driven by the voltage

$$U(t) = U_0 \cos \omega t \; . \tag{5}$$

$U(t)$ might be generated by some engine or motor. The equation governing the current $I_L(t)$ is then (e.g. Purcell, 1965):

$$L\frac{dI_L(t)}{dt} + RI_L(t) = U_0 \cos \omega t \; . \tag{6}$$

[†] Note that for logarithmic spectra the spectral density $S(f)$ is multiplied by the frequency f; therefore $fS(f) \propto f^{-2/3}$, while $S(f) \propto f^{-5/3}$.

Notice that in a mechanical context, the damping element introduced by the inductance would correspond to a friction which is proportional to velocity.

Looking only at the steady state and thus neglecting transient behavior after switching on the engine, the current oscillates at the same frequency as the driving force, with an amplitude $I_{0,L}$ and phase φ necessary to satisfy Eq. 6. The current $I_L(t)$ can then be described by

$$I_L(t) = I_{0,L}\cos(\omega t + \varphi)\ . \tag{7}$$

Substituting Eq. 7 into Eq. 6, after some algebra, yields

$$\varphi = \arctan(-\frac{\omega L}{R}) \tag{8}$$

and

$$I_{0,L} = \frac{U_0}{\sqrt{R^2 + \omega^2 L^2}}\ . \tag{9}$$

If there is no inductance L in the system (indicated by $L = 0$) and therefore no damping occurs, Eq. 9 reduces to the generally known Ohm's law

$$I_{0,L=0} = \frac{U_0}{R}\ . \tag{10}$$

According to the last two equations, the ratio between the amplitudes of the real signal and the theoretical (ideal) signal is

$$\frac{I_{0,L}}{I_{0,L=0}} = \frac{R}{\sqrt{R^2 + \omega^2 L^2}}\ . \tag{11}$$

Since the damping due to R is independent of frequency ω, we may set $R = 1$. Furthermore, we replace ω by $\omega = 2\pi f$, where f denotes the natural frequency. Thus, Eq. 11 can be written

$$\frac{I_{0,L}}{I_{0,L=0}} = \frac{1}{\sqrt{1 + 4\pi^2 f^2 L^2}}\ . \tag{12}$$

3.3. Application - The Damping of Variance and Covariance at a Single Frequency

To take advantage of the electrodynamic analogy, the driving force U is identified with the vertical wind speed of frequency ω, which forces the fluctuations in the ambient concentration of NO_2. $I_L(t)$ corresponds to the measured NO_2 concentration with the same frequency ω. The real NO_2 concentration corresponds to $I_{L=0}(t)$, which can only be obtained with an imaginary ideal measuring instrument without damping effects.

Now, the (normalized) variance of the time series $I_L(t) = I_{0,L}\cos(2\pi f t + \varphi)$ is calculated by

$$\overline{I_L'^2} = f \cdot \int_0^{1/f} I_{0,L}^2 \cos^2(2\pi f t + \varphi)\, dt = \frac{1}{2} I_{0,L}^2 \tag{13}$$

when averaged over a periodicity domain of $I_L(t)$. According to Eq. 11, the ratio of the variance for the damped and undamped time series is therefore given by

$$\frac{\overline{I_L'^2}}{\overline{I_{L=0}'^2}} = \frac{1}{1 + 4\pi^2 f^2 L^2} \propto f^{-2}\ . \tag{14}$$

Using Eq. 2 with x replaced by I_L and $I_{L=0}$, respectively, we obtain a relation between damped and undamped auto-spectrum at frequency f

$$S_{I_L}(f) = \frac{1}{1+4\pi^2 f^2 L^2} S_{I_{L=0}}(f) \; . \tag{15}$$

This explains the fact, noted at the beginning of Section 3.2, that the damped spectrum $S_{I_L}(f)$ has a proportionality factor f^{-2} greater than the undamped spectrum $S_{I_{L=0}}(f)$.

Regarding covariance, one could argue that the cospectrum of two time series, one of which is damped and one of which is not, should $\propto f^{-1}$ when compared with the undamped cospectrum. From the experimental data, however, there is strong evidence that the damped cospectrum must $\propto f^{-2}$. This can be explained in two ways: first, in an empirical way, and second by studying the behaviour of the covariance of two signals in phase (although this need not be the case for atmospheric turbulence, it could help facilitate understanding).

First, the empirical explanation is based on the description of the cospectral inertial subrange slope described by Wyngaard and Coté (1972). Using dimensional analysis, they proposed a decay $\propto f^{-7/3}$ in the inertial subrange of the cospectra of $\overline{u'w'}$ and $\overline{w'\theta'}$. For the spectra of θ and w, Kaimal *et al.* (1972) found a slope $\propto f^{-5/3}$ in the inertial subrange. Assuming that the cospectrum of w and the scalar $I_{L=0}$ is similar to the cospectrum of w and θ (Panofsky and Dutton, 1984), this leads to the empirical relation

$$Co_{w,I_{L=0}}(f) \propto f \cdot S_w(f) \cdot S_{I_{L=0}}(f) \tag{16}$$

for the inertial subrange. If the spectrum $S_{I_L}(f)$ is now damped by a factor $\propto f^{-2}$, we conclude from Eq. 16 that the cospectrum $Co_{w,I_L}(f)$ is damped by the same factor $\propto f^{-2}$ as well.

Second, the theoretical explanation leads to the missing proportionality factor of f^{-1} by considering the phase shift φ between the damped and undamped signals I_L and $I_{L=0}$, respectively. To show this, we calculate the covariance of the two time series $U(t)$ and $I_L(t)$. Recall that in the experimental context, the driving force U corresponds to the vertical wind speed w at fixed frequency $\omega = 2\pi f$, and I corresponds to the NO_2-concentration c_{NO_2} influenced by the vertical wind. According to Eq. 5 and Eq. 7, the (normalized) covariance of I_L and U is given by the integral

$$\overline{U'I'_L} = f \cdot \int_0^{1/f} U_0 \cos(2\pi f t) \cdot I_{0,L} \cos(2\pi f t + \varphi)\, dt = \frac{1}{2} U_0 I_{0,L} \cos\varphi \; . \tag{17}$$

Together with Eq. 12 the ratio of damped and undamped covariance thus becomes

$$\frac{\overline{U'I'_L}}{\overline{U'I'_{L=0}}} = \frac{I_{0,L} cos\varphi}{I_{0,L=0}} = \frac{1}{\sqrt{1+4\pi^2 f^2 L^2}} cos\varphi \; . \tag{18}$$

Note that with Eq. 8, $\cos\varphi = 1$ for $L = 0$.

We are interested in the asymptotic behaviour of Eq. 18 as a function of f. Replacing φ by Eq. 8 and setting $R = 1$ yields $\cos\varphi = \cos[\arctan(\omega L)]$, where the negative sign may be omitted due to the various symmetries. Expanding this expression into a Taylor series, centered at $\omega L = \infty$, leads to

$$\cos\varphi = \cos[\arctan(\omega L)] = \frac{1}{\omega L} - \frac{1}{2(\omega L)^3} + O(\frac{1}{\omega L})^5 \approx \frac{1}{1+\omega L} \; . \tag{19}$$

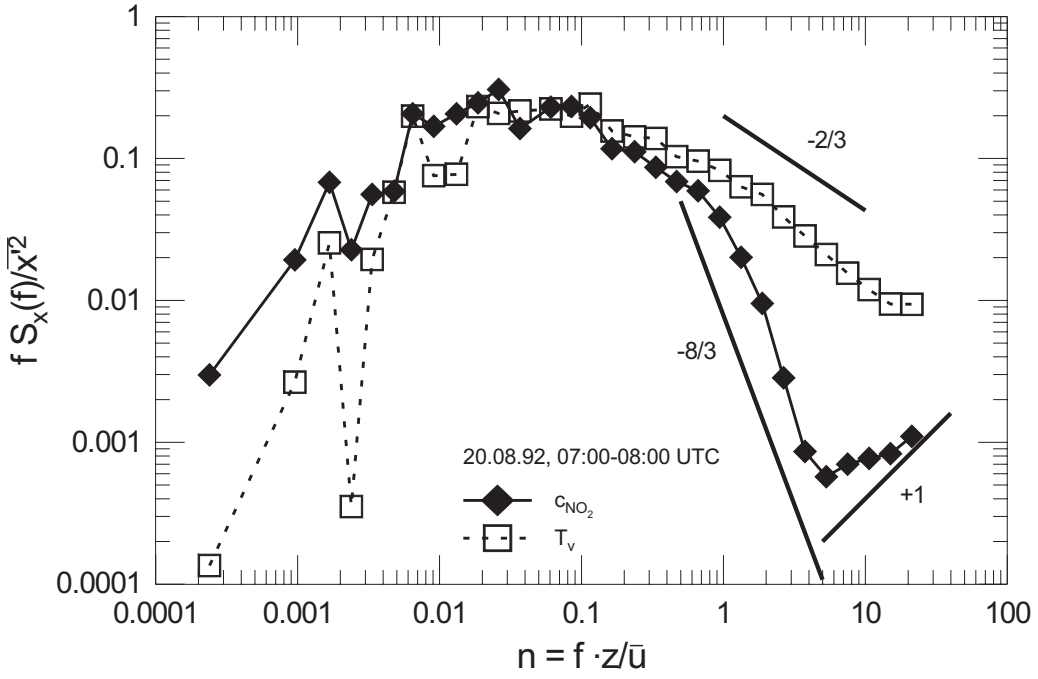

Figure 3. Spectra of virtual temperature T_v and NO_2 concentration c_{NO_2} from 20 August 1992. $\zeta = -0.37$, $z/\overline{u} = 2.4$.

For high frequencies f, the first-order approximation of Eq. 18 therefore is calculated to

$$\frac{\overline{U'I'_L}}{\overline{U'I'_{L=0}}} \approx \frac{1}{\sqrt{1+4\pi^2 f^2 L^2}} \cdot \frac{1}{1+2\pi f L} \approx \frac{1}{1+4\pi^2 f^2 L^2} \,. \tag{20}$$

Finally we apply our finding to the cospectrum of the two time series. Since by Eq. 4 we have $\overline{U'I'_L} = Co_{U,I_L}(f)$, Eq. 20 yields

$$Co_{U,I_L}(f) \approx \frac{1}{1+4\pi^2 f^2 L^2} Co_{U,I_{L=0}}(f) \,. \tag{21}$$

These equations apply to time series with one fixed frequency only. However, by the principle of superposition, they carry over to time series dependent on all frequencies $-\infty \leq f \leq \infty$. This principle will be used in the next section.

4. Results

4.1. The Damped Spectra of NO_2

Instead of I we now consider the time series $c = c_{NO_2}$ obtained from measurements as described in Section 2.2. Since the time series c contains more than one frequency, the variance $\overline{c'^2_L}$ of the damped c_{NO_2}-measurement may be written according to Eq. 1 and Eq. 15 as

$$\overline{c'^2_L} = \int_0^\infty S_{c_L}(f)\, df = \int_0^\infty \frac{1}{1+4\pi^2 f^2 L^2} S_{c_{L=0}}(f)\, df \tag{22}$$

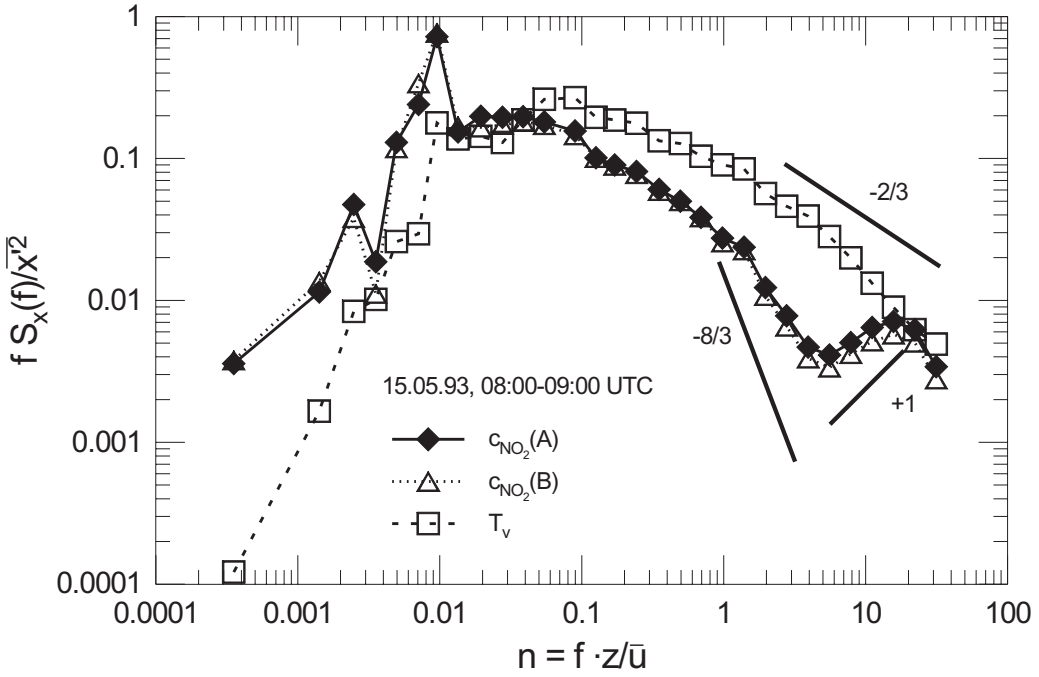

Figure 4. Spectra of virtual temperature T_v and NO_2 concentration c_{NO_2} from 15 May 1993. $\zeta = -0.78$, $z/\overline{u} = 3.5$. Spectra of two similar NO_2 analysers, labeled (A) and (B), are shown.

where $c_{L=0}$ denotes the undamped NO_2-concentration.

Since $S_{c_{L=0}}(f) \propto f^{-5/3}$ (Kaimal *et al.*, 1972), the new damped spectrum $S_{c_L}(f)$ (Eq. 22) is expected to show a proportionality to $f^{-5/3} \cdot f^{-2}$ in the inertial subrange, which $\propto f^{-8/3}$ in the logarithmic plot of Fig. 4.1 and 4. This behaviour agrees with experimental data in Fig. 4.1 and Fig. 4, if the contribution from white noise ($\propto f^{+1}$) is neglected: In Fig. 4.1 the spectrum of T_v obeys the $f^{-2/3}$ power law in the inertial subrange, and the spectrum of NO_2 obeys the $f^{-8/3}$ law expected from Eq. 22. The white noise is clearly visible in the NO_2 spectrum, and even the T_v spectrum shows a weak bend towards the f^{+1} slope near the cut-off frequency. In Fig. 4 the two different proportionalities are visible as well, but both NO_2 spectra from two parallel-driven LMA-3 show a continuous transition from damped slope to white noise slope. Nevertheless, the damping law $\propto f^{-2}$ is very clear in the corresponding cospectra in Fig. 6, indicating that the cospectra are quite inert to noise in the original time series (Hicks and McMillen, 1988).

Unfortunately, the damping of the instrument depends on the (natural) frequency f, while the shape of the spectrum depends on the non-dimensional Monin-Obukhov stability parameter ζ (Monin and Obukhov, 1954) and the non-dimensional frequency n. n is related to f by $z/\overline{u}$:

$$n = fz/\overline{u}\ . \tag{23}$$

Therefore, four independent variables ζ, f, z, $\overline{u}$, plus the system damping constant L, are used in the correction model in Section 4.3.

4.2. The Damped Cospectra of the Vertical Flux of NO_2

In Section 4.1 it was stated that the white noise alters the shape of the spectra at higher frequencies. This is not the case with the cospectra. The white noise contribution of the

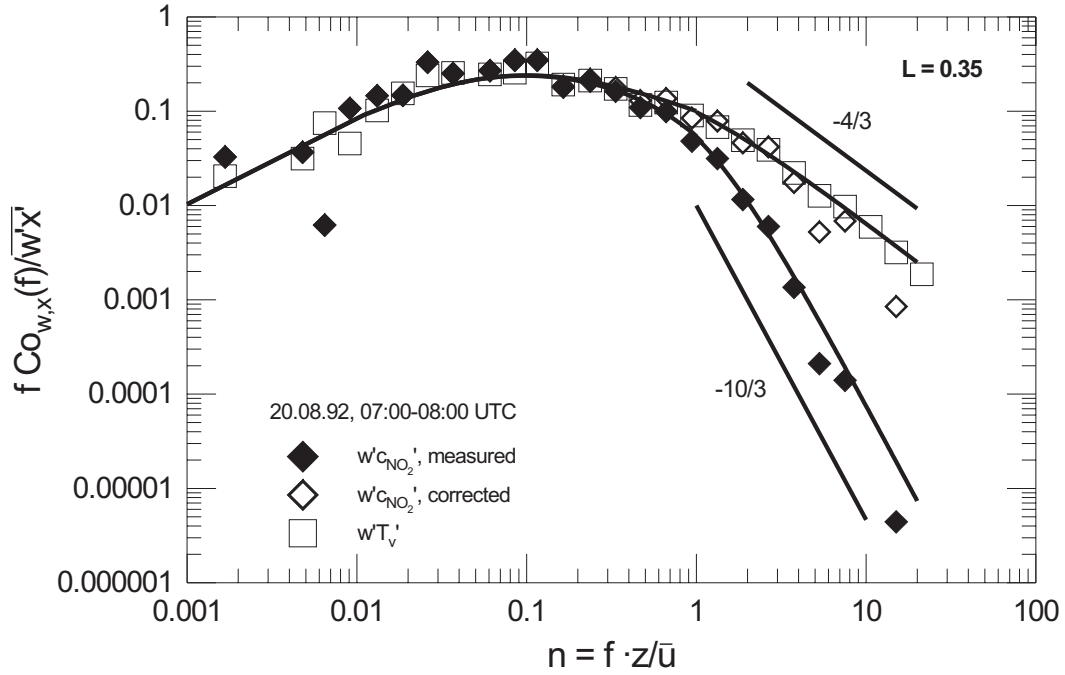

Figure 5. Cospectra of virtual heat flux $\overline{w'T_v'}$ and vertical turbulent NO_2 flux $\overline{w'c'_{NO_2}}$ from 20 August 1992. $\zeta = -0.37$, $z/\overline{u} = 2.4$, $L = 0.35$.

NO_2 time series is not correlated with the vertical wind speed as stated in Hicks and McMillen(1988). Examples of such cospectra are given in Fig. 5 and Fig. 6.

The proportionality expected from Eq. 21 is also in good agreement with the experimental cospectra. Therefore, setting $Co_{w,c_L} = \frac{1}{1+4\pi^2 f^2 L^2} \cdot Co_{w,c_{L=0}}$, the superposition of all frequencies with Eq. 3 yields

$$\overline{w'c'_L} = \int_0^\infty Co_{w,c_L}(f)\, df = \int_0^\infty \frac{1}{1+4\pi^2 f^2 L^2} Co_{w,c_{L=0}}(f)\, df \tag{24}$$

for the covariance of the measured (i.e. damped) NO_2 flux.

In Fig. 5 the empirical formula of Kaimal *et al.* (1972), which will be given in Section 4.3, fits the cospectrum of $\overline{w'T_v'}$ quite well (upper curve), while the modified version (Eq. 24) fits the cospectrum $\overline{w'c'_{NO_2}}$ when the inductance L is given a value of 0.35. In May 1993 an inductance of 0.3 fit the damped cospectra in Fig. 6 best. The large scatter at high frequencies appears exaggerated according to the double logarithmic plot of Fig. 6. To obtain area constancy, the high frequency part of Fig. 6 is plotted with a linear ordinate in Fig. 7, illustrating that sign reversals and scatter are unimportant for the total covariance. In Fig. 7 the area between the two model fits corresponds to the damping loss of the NO_2 flux measurements. This damping loss can be calculated with the correction model presented in the following section.

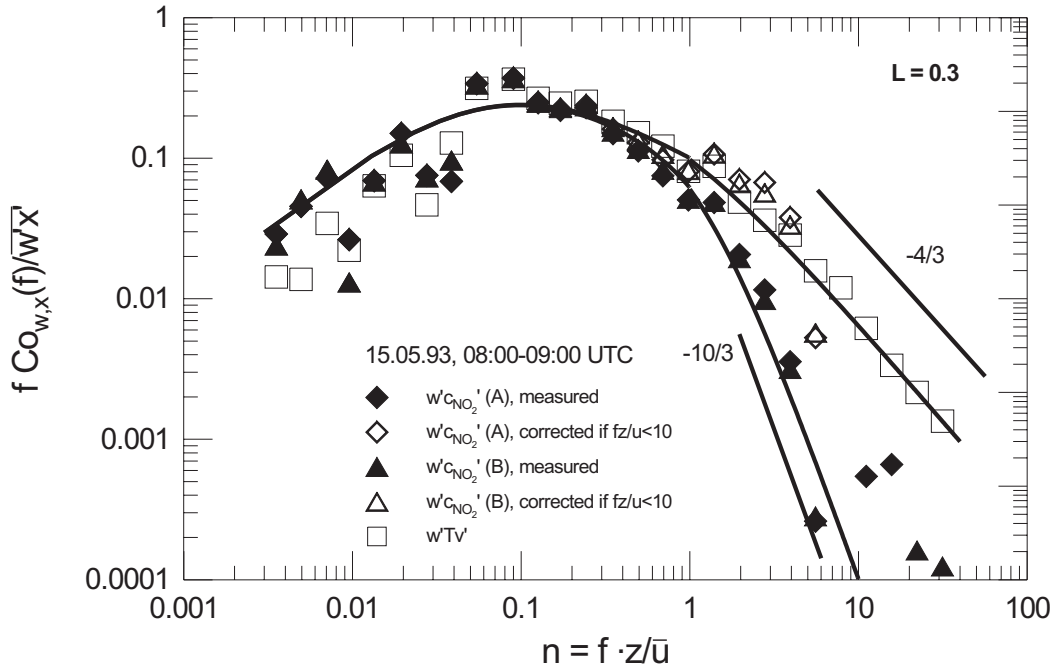

Figure 6. Cospectra of virtual heat flux $\overline{w'T'_v}$ and vertical turbulent NO_2 flux $\overline{w'c'_{NO_2}}$ from 15 May 1993. $\zeta = -0.78$, $z/\overline{u} = 3.5$, $L = 0.3$.

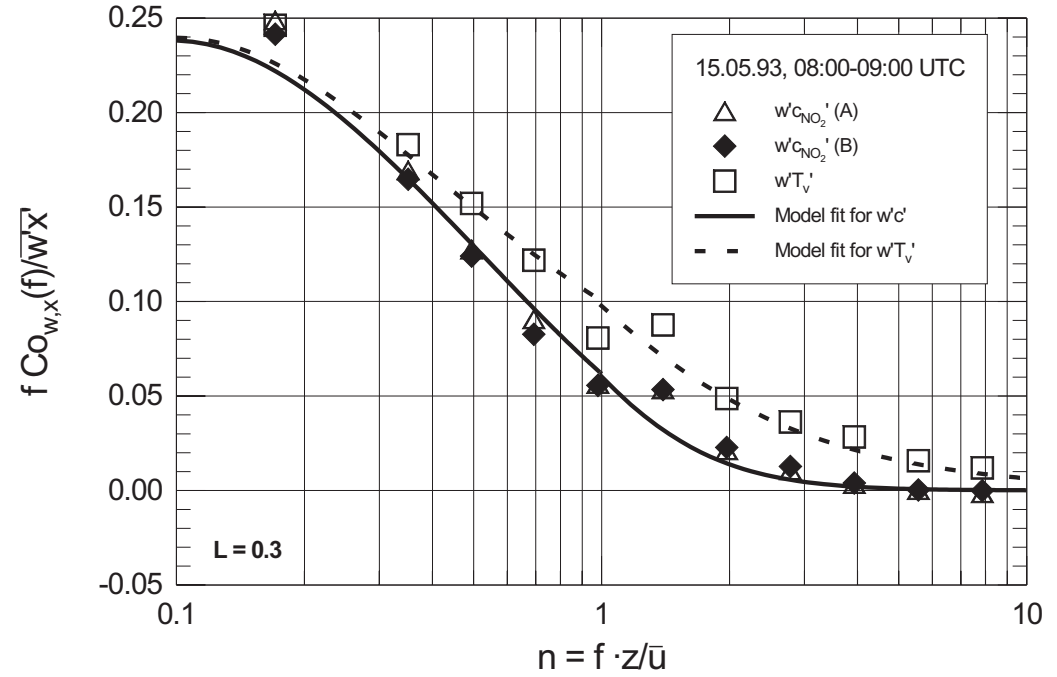

Figure 7. High frequency damping in the cospectra of vertical turbulent NO_2 flux $\overline{w'c'_{NO_2}}$ from 15 May 1993. In this plot areas are proportional to the respective cospectral densities.

4.3. THE COSPECTRAL CORRECTION MODEL FOR THE VERTICAL FLUX OF NO_2 AND OTHER SCALARS

In order to calculate the theoretical (i.e. undamped) cospectrum $Co_{w,c_{L=0}}(f)$, we started with the empirical formula proposed by Kaimal *et al.* (1972) for $\overline{w'\theta'}$. To guarantee that

$$\int_0^\infty \frac{f\,Co_{w,c_{L=0}}(f)}{\overline{w'c'_{L=0}}}\,d(\log f) = 1.0\;, \tag{25}$$

a slight modification of the parameters in this formula was needed. For unstable and neutral stratification ($-2 \le \zeta \le 0$), the formula after the correction reads:

$$\frac{fCo_{w,c_{L=0}}(f)}{\overline{w'c'_{L=0}}} = \left\{ \begin{array}{ll} 10.53n/(1+13.3n)^{1.75}, & n \le 1.0 \\ 4.21n/(1+3.8n)^{2.4}, & n \ge 1.0 \end{array} \right\}, -2 \le \zeta \le 0\;. \tag{26}$$

Recall that $n = f \cdot z/\overline{u}$. For stable stratification ($0 < \zeta \le 2$), the cospectrum calculated by Kaimal *et al.* (1972) was adapted to

$$\frac{fCo_{w,c_{L=0}}(f)}{\overline{w'c'_{L=0}}} = \frac{0.81(n/n_0)}{1+1.5(n/n_0)^{2.1}}, \quad 0 < \zeta \le +2\;, \tag{27}$$

with

$$n_0 = \left\{ \begin{array}{ll} 0.23, & -2 \le \zeta \le 0 \\ 0.23(1+6.4\zeta)^{3/4}, & 0 \le \zeta \le +2 \end{array} \right\}\;. \tag{28}$$

The damped cospectra can be derived by combining Eq. 24 with Eq. 26 and Eq. 27, respectively. For unstable and neutral stratification, the normed cospectrum of the measured NO_2 fluxes was modified to

$$\frac{fCo_{w,c_L}(f)}{\overline{w'c'_{L=0}}} = \left\{ \begin{array}{ll} 10.53n/[(1+4\pi^2f^2L^2)(1+13.3n)^{1.75}], & n \le 1.0 \\ 4.21n/[(1+4\pi^2f^2L^2)(1+3.8n)^{2.4}], & n \ge 1.0 \end{array} \right\}, -2 \le \zeta \le 0\;, \tag{29}$$

while for stable stratification the normed cospectrum was modified to

$$\frac{fCo_{w,c_L}(f)}{\overline{w'c'_{L=0}}} = \frac{1}{1+4\pi^2f^2L^2} \cdot \frac{0.81(n/n_0)}{1+1.5(n/n_0)^{2.1}}\;, \quad 0 < \zeta \le 2\;. \tag{30}$$

Next, we defined ξ to be the ratio between the damped covariance of NO_2 flux and the undamped effective covariance. Thus ξ is given by

$$\xi = \frac{\overline{w'c'_L}}{\overline{w'c'_{L=0}}} = \int_0^\infty \frac{f\,Co_{w,c_L}(f)}{\overline{w'c'_{L=0}}}\,d(\log f)\;. \tag{31}$$

In other words, the measurable fraction ξ of the covariance was obtained by integrating Eq. 29 for unstable and neutral conditions and by integrating Eq. 30 for stable conditions, respectively. Lacking an analytical solution in unstable and neutral conditions, we approximated

$$\xi \approx \alpha \cdot \arctan\left[\beta \cdot \ln\left(\frac{z}{\overline{u} \cdot L} + 1\right) + \gamma\right], \quad -2 \le \zeta \le 0 \tag{32}$$

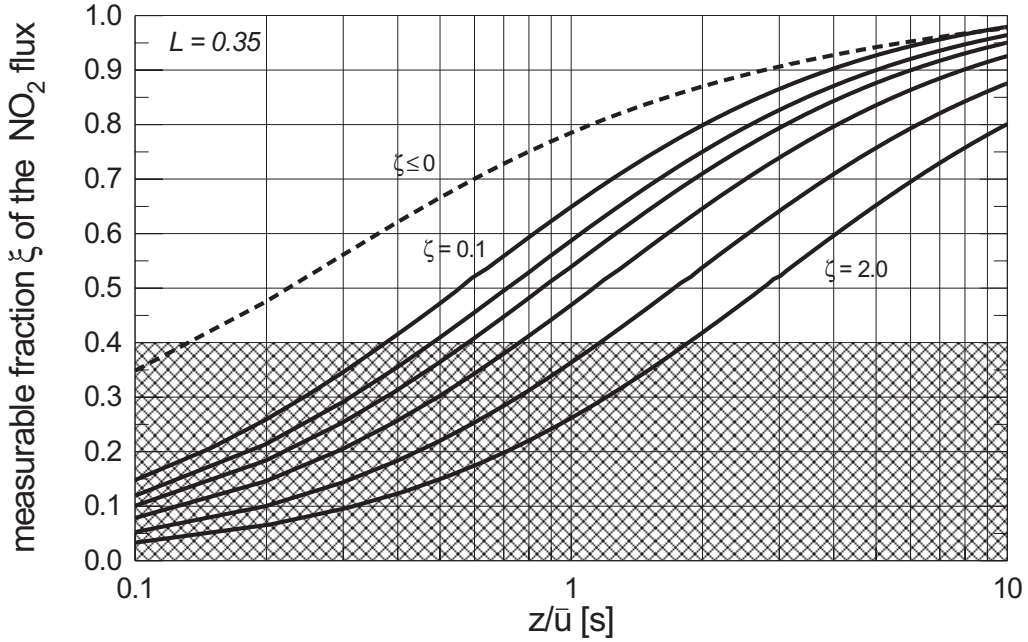

Figure 8. Fraction ξ of the NO_2 flux which can be measured with a damped instrument. Example for $L = 0.35$. Broken line: unstable and neutral stratification (Eq. 32); solid lines: stable stratification with $\zeta = 0.1$, 0.2, 0.3, 0.5, 1.0, 2.0 (Eq. 33).

by a least squares fit to the numerical integral of the damped cospectrum. Since ξ depends on the damping due to chemical analysing instruments, it lies within a range between 1.0 (no damping at all) and 0.0 (no signal at all). The fit was restricted to the range $0.4 \leq \xi \leq 1.0$. The best fit was evaluated for a range of inductances $0.25 \leq L \leq 1.0$ which was appropriate for the LMA-3 instruments. The coefficients determined in this way were $\alpha = 0.725$, $\beta = 1.24$ and $\gamma = 0.21$. In practice, all measurements with $\xi < 0.40$ were discarded.

For stable conditions (Eq. 30), an analytical solution to the integration can be found if the exponent of 2.1 is replaced by 2.0. This modification gives a surplus of theoretical covariance (i.e. when $L = 0$) in the order of 3.9 percent. Therefore, the result of the integration of Eq. 30 was normalized by 1.039 to yield $\xi = 1.0$ for $L = 0$. Using this modification, the fraction ξ of the total covariance which can be measured with a damped instrument can be calculated by

$$\xi \approx \frac{3}{\sqrt{6}} \cdot \frac{z}{\overline{u}} \cdot \frac{\sqrt{6} \cdot z/\overline{u} - 4\pi L n_0}{3(z/\overline{u})^2 - 8\pi^2 L^2 n_0^2}, \quad 0 < \zeta \leq 2\,. \tag{33}$$

In the field, the values of z and L do not vary significantly as long as the measuring system is not altered (e.g. by attaching a new teflon tube to the LMA-3). The sonic anemometer measures $\overline{u}$ and ζ simultaneously with the NO_2 flux.

Eq. 32 and Eq. 33 are shown in Fig. 8 for $L = 0.35$, determined from the data for August and September 1992. In the region where $\xi < 0.40$ (shaded area in Fig. 8), Eq. 32 and Eq. 33 still fit the numerically integrated curves (not shown in this Fig.) quite well, but from the experimental point of view it is not recommended to use measurements which represent less than 40 percent of the real fluxes.

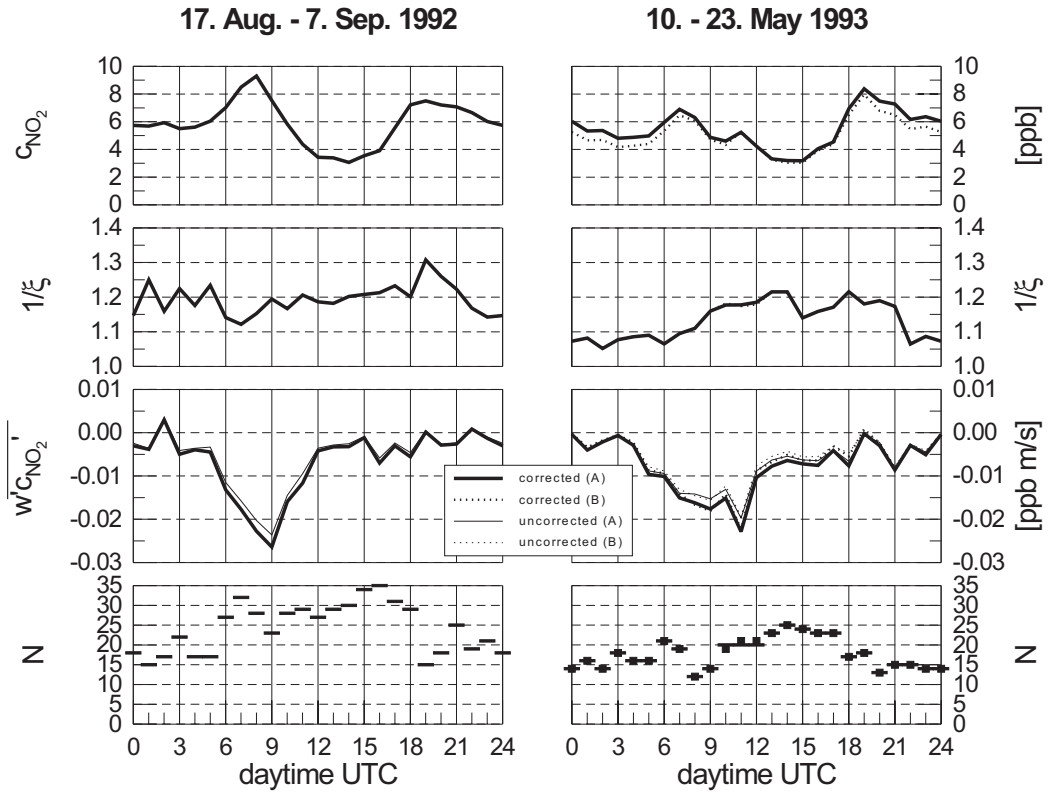

Figure 9. Averaged diurnal cycles of NO_2 concentration c_{NO_2}, correction factor $1/\xi$, NO_2 flux $\overline{w'c'_{NO_2}}$ (measured: fine lines; and corrected: bold lines) and number of samples N (30 minute averages aggregated to hourly values). In the data for May, solid lines and horizontal bars correspond to the measurements obtained from one LMA-3 (A), dotted lines and squares from another LMA-3 (B).

Table III. Correction factors $1/\xi$ for unstable and neutral stratification (Eq. 32) and different instrumental inductances L. Numbers in italics show that $\xi < 0.40$.

$L =$		0.25	0.30	0.35	0.40	0.45	0.50	0.75	1.0
$z/\overline{u} =$	0.1	2.462	*2.675*	*2.869*	*3.045*	*3.206*	*3.354*	*3.939*	*4.350*
	0.2	1.830	1.969	2.101	2.227	2.348	2.462	*2.959*	*3.354*
	0.5	1.373	1.438	1.501	1.563	1.624	1.684	1.969	2.227
	1	1.204	1.240	1.274	1.307	1.341	1.373	1.532	1.684
	2	1.110	1.130	1.150	1.168	1.187	1.204	1.291	1.373
	5	1.041	1.052	1.062	1.071	1.080	1.089	1.130	1.168
	10	1.010	1.017	1.023	1.030	1.035	1.041	1.066	1.089

Since by definition $\overline{w'c'_{L=0}} = \frac{1}{\xi}\overline{w'c'_L}$, (cf. Eq. 31), the reciprocal $\frac{1}{\xi}$ of ξ is interpreted as a correction factor for the measured covariance $\overline{w'c'_L}$. In Tab. III correction factors for different L are shown for unstable and neutral stratification (Eq. 32 used). Usually, peak NO_2 flux occurs during the daytime when atmospheric stratification is unstable (Fig. 9).

Fig. 9 shows mean daily cycles of the NO_2 concentrations, the correction factors $1/\xi$, the NO_2 fluxes, and the number of measurements (30 minute averages, aggregated to

hourly means). In August and September 1992 the daily average of the correction factor was 1.20 (range 1.12–1.31), in May 1993 it was 1.14 (1.05–1.22). For the three hours of peak NO_2 flux, the correction factors are similar in both periods: 1.17 in August and September 1992 (peak NO_2 flux at 9 UTC) and 1.18 in May 1993 (peak NO_2 flux at 11 UTC).

5. Final Comments and Conclusions

The cospectral correction model discussed here is intended to reconstruct the part of the real turbulent NO_2 flux which cannot be measured with an imperfect NO_2 sensor. Even though the model was developed using NO_2 data from a Luminox LMA-3 instrument, it can also be applied to measurements obtained by any chemical sensor that shows a frequency-dependent damping in the spectrum and cospectrum of the time series. The correction model relies on the cospectral similarity (Panofsky and Dutton, 1984) of vertical turbulent scalar fluxes. The flux itself is measured using the eddy correlation technique. It is assumed that the vertical wind speed measurements w are correct and only the sensor for the measurements of concentration c is damped (imperfect sensor; Hicks and McMillen, 1988). The damping of the measurement can then be described by an analogy to inductance in an alternating current circuit. The inductance of the measuring instrument is a result of the inlet system (non-turbulent flux in the teflon tube attached to the inlet pump) and the slow wet-chemical reaction of NO_2 with the Luminol solution. It can be expected that in other instruments with direct optical measurement of c, the only damping effect would be the one caused by a long aspiration tube. The problem of damping could possibly be partly overcome with a powerful pump which keeps the flow turbulent in the inlet system (e.g. Pilegaard *et al.*, 1993). Nevertheless, a large air flow volume in the inlet system would require a large spatial separation between tube inlet and sonic anemometer head, leading to another loss of covariance (see Moore, 1986, for the specific contributions of the diverse parts of a measuring instrument to total damping). Only direct comparison experiments can show which approach is more exact with regard to measured eddy fluxes. With the correction model proposed here, measured NO_2 fluxes were corrected by a factor of 1.05 to 1.31. This factor was calculated as a function of measuring height z above zero-displacement, instrumental inductance L (both more or less constant for a specific measuring phase where the systems are not altered), mean horizontal wind speed $\overline{u}$, and Monin-Obukhov stability ζ (variables). During the time with the largest negative NO_2 fluxes, the correction factors were virtually the same in both field campaigns (1.17 in August and September 1992, 1.18 in May 1993).

Acknowledgements

This study was funded by The Swiss Federal Office for Environment, Forests and Landscape, grant FE/BUWAL/310.90.81. We wish to thank Drs. Albrecht Neftel and Rolf Hesterberg from The Swiss Federal Research Station for Agricultural Chemistry and Environmental Hygiene (Liebefeld-Bern) for the NO_2 measurements used in this work. The authors are indebted to Prof. Heinz Wanner (Bern, Switzerland) for coordination of the project and to Dr. Jørgen Højstrup (Risø, Denmark) and Dr. Hans-Peter Schmid (Zürich, Switzerland) for their valuable comments on the manuscript.

References

Businger, J. A.: 1986, 'Evaluation of the Accuracy with which Dry Deposition can be Measured with Current Micrometeorological Techniques', *J. Climate and Appl. Meteorol.* **25**, 1100–1124.

Claussen, M.: 1985, 'A Model of Turbulence Spectra in the Atmospheric Surface Layer', *Boundary-Layer Meteorol.* **33**, 151–172.

Grant, A. L. M. and R. D. Watkins: 1989, 'Errors in Turbulence Measurements with a Sonic Anemometer', *Boundary-Layer Meteorol.* **46**, 181–194.

Ellenberg, H.: 1990, 'Ökologische Veränderungen in Biozönosen durch Stickstoffeintrag', *In: Ammoniak in der Umwelt – Kreisläufe, Wirkungen, Minderung*, Darmstadt: Kuratorium für Technik und Bauwesen in der Landwirtschaft, 44.1–44.24.

Hesterberg, R.: 1994, 'Die Stickoxide im schweizerischen Mittelland und der Stickstoffeintrag in ein Naturschutzgebiet', *PhD-Thesis* University of Bern (unpublished).

Hesterberg, R., A. Blatter, M. Fahrni, M. Rosset, A. Neftel, W. Eugster and H. Wanner: 1995, 'Deposition of Nitrogen-Containing Compounds to a Non-Cultivated Area in Central Switzerland', *Environmental Pollution,accepted for publication*.

Hicks, B. B. and R. T. McMillen: 1988, 'On the Measurement of Dry Deposition using Imperfect Sensors and in Non-Ideal Terrain', *Boundary-Layer Meteorol.* **42**, 79–94.

Højstrup, J.: 1981, 'A Simple Model for the Adjustment of Velocity Spectra in Unstable Conditions Downstream of an Abrupt Change in Roughness and Heat Flux', *Boundary-Layer Meteorol.* **21**, 341–356.

Kaimal, J. C. and J. E. Gaynor: 1991, 'Another Look at Sonic Thermometry', *Boundary Layer Meteorol.* **56**, 401–410.

Kaimal, J. C. and J. E. Gaynor: 1983, 'The Boulder Atmospheric Observatory', *J. Climate and Appl. Meteorol.* **22**, 863–880.

Kaimal, J. C., J. C. Wyngaard and D. A. Haugen: 1968, 'Deriving Power Spectra from a Three-Component Sonic Anemometer', *J. Appl. Meteorol.* **7**, 827–837.

Kaimal, J. C., J. C. Wyngaard, Y. Izumi and O. R. Coté: 1972, 'Spectral Characteristics of Surface-Layer Turbulence', *Quart. J. Roy. Meteorol. Soc.* **98**, 563–589.

Leuning, R. and J. Moncrieff: 1990, 'Eddy-Covariance CO_2 Flux Measurements Using Open- and Closed-Path CO_2 Analysers: Corrections for Analyser Water Vapour Sensitivity and Damping of Fluctuations in Air Sampling Tubes', *Boundary-Layer Meteorol.* **53**, 63–76.

Monin, A. S. and A. M. Obukhov: 1954, 'Osnovnye zakonomernosti turbulentnogo peremešivaniâ v prizemnom sloe atmosfery', *Trudy geofiz. inst. Akad. Nauk SSSR* **24 (151)**, 163–187.

Moore, C. J.: 1986, 'Frequency Response Corrections for Eddy Correlation Systems', *Boundary-Layer Meteorol.* **37**, 17–35.

Panofsky, H. A.: 1978, 'Matching in the Convective Planetary Boundary Layer', *J. Atmos. Sci.* **35**, 272–276.

Panofsky, H. A. and J. A. Dutton: 1984, 'Atmospheric Turbulence', New York: John Wiley & Sons.

Panofsky, H. A., D. Larko, R. Lipschutz, G. Stone, E. F. Bradley, A. J. Bowen and J. Højstrup: 1982, 'Spectra of Velocity Components over Complex Terrain', *Quart. J. Roy. Meteorol. Soc.* **108**, 215–230.

Philip, J. R.: 1963a, 'The Theory of Dispersal during Laminar Flow in Tubes. II', *Aust. J. Phys.* **16**, 300–310.

Philip, J. R.: 1963b, 'The Damping of a Fluctuating Concentration by Continuous Sampling through a Tube', *Aust. J. Phys.* **16**, 454–463.

Pilegaard, K., P. Hummelshøj and N. O. Jensen: 'Deposition of Ozone and Nitrogen Dioxide to Open Land and Forests', *Contribution to the BIATEX Workshop Aveiro, May 1993*, 1–8.

Purcell, E. M.: 1965, 'Electricity and Magnetism', *Berkeley Physics Course* **2**, New York: McGraw–Hill Book, 274–295.

Skupniewicz, C. E., R. F. Kamada and G. E. Schacher: 1989, 'Turbulence Measurements over Complex Terrain', *Boundary-Layer Meteorol.* **48**, 109–128.

Vilá-Guerau de Arellano, J. and P. G. Duynkerke: 1992, 'Influence of Chemistry on the Flux-Gradient Relationship for the NO-O_3-NO_2 System', *Boundary-Layer Meteorol.* **61**, 375–387.

Wyngaard, J. C. and O. R. Coté: 1972, 'Cospectral Similarity in the Atmospheric Surface Layer', *Quart. J. R. Met. Soc.* **98**, 590–603.

Zeman, O. and N. O. Jensen: 1987, 'Modification of Turbulence Characteristics in Flow over Hills', *Quart. J. Roy. Meteorol. Soc.* **113**, 55–80.